2990–3000 *Nucleic Acids Research, 2008, Vol. 36, No. 9* *Published online 3 April 2008*
doi:10.1093/nar/gkn156

The poly(A) site sequence in HDV RNA alters both extent and rate of self-cleavage of the antigenomic ribozyme

Abigail L. Brown, Anne T. Perrotta, Timothy S. Wadkins and Michael D. Been*

Department of Biochemistry, Duke University Medical Center, Durham NC 27710, USA

Received November 28, 2007; Revised March 18, 2008; Accepted March 19, 2008

ABSTRACT

The ribozyme self-cleavage site in the antigenomic sequence of hepatitis delta virus (HDV) RNA is 33-nt downstream of the poly(A) site for the delta antigen mRNA. An HDV antigenomic ribozyme precursor RNA that included the upstream poly(A) processing site was used to test the hypothesis that nonribozyme sequence near the poly(A) site could affect ribozyme activity. Relative to ribozyme precursor without the extra upstream sequences, the kinetic profile for self-cleavage of the longer precursor was altered in two ways. First, only half of the precursor RNA self-cleaved. The cleaved fraction could be increased or decreased with mutations in the upstream sequence. These mutations, which were predicted to alter the relative stability of competing secondary structures within the precursor, changed the distribution of alternative RNA structures that are resolved in native-gel electrophoresis. Second, the active fraction cleaved with an observed rate constant that was higher than that of the ribozyme without the upstream sequences. Moreover, the higher rate constants occurred at lower, near-physiological, divalent metal ion concentrations (1–2 mM). Modulation of ribozyme activity, through competing alternative structures, could be part of a mechanism that allows a biologically significant choice between maturation of the mRNA and processing of replication intermediates.

INTRODUCTION

Hepatitis delta virus (HDV), a single-stranded RNA satellite of the hepatitis B virus, is proposed to replicate its RNA genome by a double rolling-circle mechanism (1–3). In this model for replication, RNA synthesis generates longer-than-unit-length products that are processed by a *cis*-cleaving ribozyme in each strand to yield monomer-length antigenomic and genomic RNAs. These linear monomers are circularized and serve as templates for additional rounds of replication. In addition to serving as a template for replication, the genomic RNA strand is the template for the transcription of an mRNA for the delta antigens. In this mRNA, the poly(A) site is 33-nt upstream of the ribozyme cleavage site (4,5). Thus, the two processing sites are very close to each other, and, yet, these alternative processing paths must be distinct since a polyadenylated product cannot serve as a template for replication and ribozyme cleavage would be predicted to interfere with mRNA maturation (6,7).

Models for replication and mRNA transcription in HDV that use either different cellular RNA polymerases (8) or different forms of the same polymerase (9) are attractive because RNA processing is closely linked to RNA synthesis (10,11). Two models that can account for both rolling-circle replication and mRNA synthesis using the same genomic strand of HDV RNA as template come from the labs of Lai (8) and Taylor (9). In one model, it is proposed that RNA Pol II transcribes the delta antigen mRNA and RNA Pol I synthesizes the full-length antigenomic replication product (8,12). In other models, however, RNA Pol II synthesizes both forms of the antigenomic RNA sequence. In a recent paper from the Taylor group (9), it is proposed that RNA Pol II initiates synthesis at a single promoter region in the folded genomic RNA. The resulting transcript can be polyadenylated to generate the mRNA or processed at the ribozyme site to generate the replication intermediate, but not both. This model differs from an earlier model where they suggested that a single Pol II initiation could first yield a polyadenylated mRNA, and then, by not terminating, continue synthesis to yield ribozyme-processed full-length products (5). Nevertheless, in all of these proposed models, RNA Pol II is responsible for synthesis of the mRNA, and therefore, ribozyme self-cleavage in that transcript could interfere with its polyadenylation.

*To whom correspondence should be addressed. Tel: +1 91 9684 2858; Email: mike.been@duke.edu
Present address:
Timothy S. Wadkins, Victory Brewing Co., Downingtown, PA 19335, USA

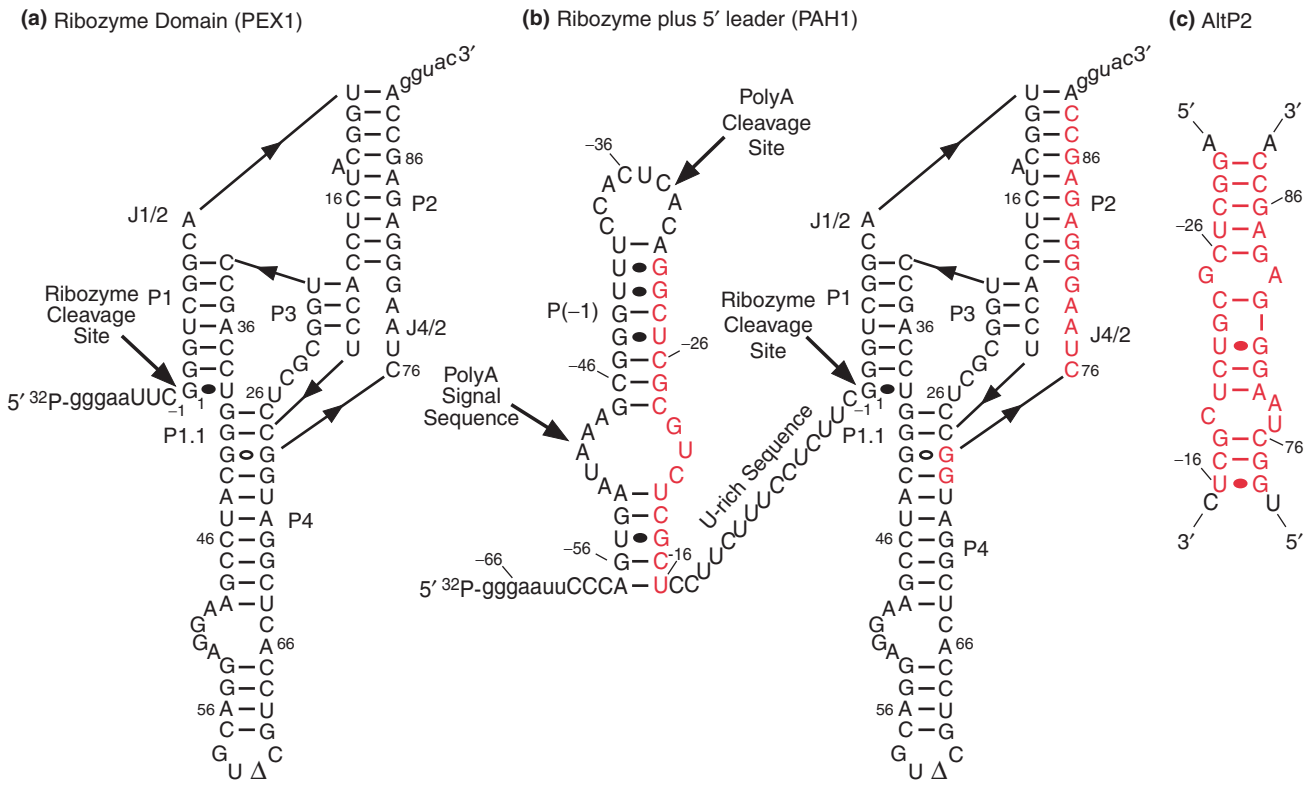

Figure 1. Sequence and secondary structure of the self-cleaving domain of the antigenomic HDV ribozyme. (**a**) PEX1, lowercase letters indicate vector-derived sequence. (**b**) PAH1 with the upstream sequences drawn in a hypothetical P(-1) hairpin stem–loop. Nucleotide numbering begins from the ribozyme cleavage site with negative values for the 5′ sequences. Poly(A) sequence elements, the AAUAAA hexamer, the cleavage/polyadenylation site at −33 (4), and the U-rich region between P(-1) and P1 are labeled. (**c**) A proposed alternative pairing designated as AltP2.

Here, we test if the close proximity of the poly(A) site and the ribozyme could allow sequence interactions between the two regions to influence the choice between ribozyme cleavage and polyadenylation.

In vitro studies of the HDV antigenomic ribozyme and its catalytic mechanism have focused on the activity of a small, or minimal, cleavage domain (Figure 1a). This form of the ribozyme does not include the upstream poly(A) signals. However, there was early evidence that sequences 5′ to the cleavage site could affect HDV ribozyme activity (13,14). Subsequently, Chadalavada *et al.* (15,16) more thoroughly investigated and characterized the effect of upstream nonribozyme sequence on genomic HDV ribozyme activity. In those studies, they identified both a base-pairing interaction between the upstream sequence and the ribozyme sequence (Alt 1) and a competing hairpin within the upstream sequence [P(-1)] that would interfere with Alt 1 formation.

The HDV poly(A) site is comprised of sequence elements that are similar to those found in cellular mRNAs (11,17).These sequence elements consist of the highly conserved AAUAAA hexamer, which is recognized by the cleavage and polyadenylation-specificity factor (CPSF), potential CA cleavage sites downstream of the AAUAAA sequence, and a U-rich sequence downstream of the CA sites that could function as a binding site for the cleavage stimulation factor (CstF). These sequences also have the potential to be included in secondary structures resembling those noted for the genomic ribozyme (18). They could form both a hairpin, P(-1), involving nucleotides −57 to −16 (numbering is relative to the ribozyme cleavage site) (Figure 1b), and an alternative pairing of nucleotides −30 to −12 in the upstream sequence with nucleotides 74–88 of J4/2 and the 3′ side of P2 in the ribozyme (Figure 1c). This alternative pairing is similar to the pairing in the genomic sequence called Alt 1 (16), but here we called it AltP2 following a nomenclature similar to that used by Pan and Woodson (19) for the Group I intron. As described for the genomic sequence, the 5′ side of AltP2 and the 3′ side of P(-1) share a common sequence, so only one of the two pairings is presumed to form in a transcript. For the antigenomic RNA sequence, an AltP2-like (Alt 1, in the genomic ribozyme) interaction would prevent ribozyme cleavage, while a P(-1)-like structure might reduce the efficiency of polyadenylation (20–22).

To examine the effect that the upstream polyadenylation sequences might have on ribozyme activity, the antigenomic ribozyme construct PEX1 was modified by the addition of 60 nt of wild-type sequence 5′ to the cleavage site to generate the precursor PAH1 (Figure 1b). Both the ribozyme and upstream sequences were based on HDV isolate US-2 (ID 261991). We report here that this longer construct formed at least two different folded populations, in about equal amounts, which could be physically separated. One population cleaved rapidly while the other did not cleave to any appreciable level under the same conditions. Mutations that favored one proposed fold over the other changed the amount of

cleaved RNA in a predictable manner. Somewhat unexpectedly, the observed cleavage rate for the cleavable fraction with the longer precursors was greater than that for precursors containing only the ribozyme domain. These results suggested that the 5′ sequences inhibited cleavage activity in one folded population but may have enhanced the cleavage rate of the other population.

MATERIALS AND METHODS

Enzymes and reagents

T7 RNA polymerase was purified by M. Puttaraju from an overexpressing clone provided by W. Studier (23). Oligonucleotides were ordered from Integrated DNA Technologies. Other enzymes and chemical supplies were purchased from commercial sources.

Plasmids

The plasmid pPAH1 was prepared by inserting a synthetic double-stranded DNA containing 149 nt of wild-type HDV sequence into the plasmid pTZ18R; it contains both the antigenomic HDV core ribozyme sequence present in PEX1 (24) and a 60-nt sequence upstream of the ribozyme cleavage site. This DNA duplex was constructed using three pairs of oligonucleotides that were annealed, ligated and inserted into EcoRI and BanI cut plasmid. The DNA was transformed into *Escherichia coli* (JM83), and the correct DNA sequence was confirmed by sequencing miniprep DNA as previously described (25). Plasmid DNA for transcriptions was prepared from 250-ml cultures and purified by CsCl equilibrium density ultracentrifugation with ethidium bromide. Variants of PAH1 were made by oligonucleotide-directed mutagenesis of a uracil-containing single-stranded pPAH1 template (26–28). Plasmid DNA for each mutant was prepared as described above.

Transcriptions

Transcription of BanI cut plasmid DNA with T7 RNA polymerase yielded the 149-nt PAH1 sequence with 7-nt and 5-nt vector-derived sequences at the 5′ and 3′ ends, respectively. RNA for ribozyme cleavage reactions was made in transcription reactions (25 µl, 15 min, 37°C) that contained 40 mM Tris–HCl (pH 7.5), 15 mM $MgCl_2$, 5 mM dithiothreitol, 2 mM spermidine, 1 mM each ATP, UTP and GTP, 0.5 mM CTP, 6 µg DNA, 25 µCi [α^{32}P]-CTP and 300 U T7 RNA polymerase. Reactions were terminated with an equal volume of formamide stop mix containing 100 mM EDTA, and the products were separated by electrophoresis on a 6% polyacrylamide gel containing 7 M urea. Following electrophoresis, precursor RNA was located by autoradiography and excised from the gel. RNA was eluted in 0.1% SDS and 1 mM EDTA, desalted by G25 gel-filtration, ethanol precipitated and stored in 0.1 mM EDTA at −20°C. To prepare unlabeled RNA, the volume of the transcription reaction was increased to 75 µl, and the RNA was located by UV shadowing after gel electrophoresis.

Ribozyme cleavage assays

For the hand-mixing experiments, radiolabeled precursor RNA in 0.1 mM EDTA was heated at 95°C for 3 min and cooled to room temperature. The buffer conditions were adjusted to 40 mM Tris–HCl (pH 7.5), 1 mM EDTA, 0.5 mM spermidine (TES), and the RNA was preincubated at 37°C for 15 min followed by 25°C for 10 min. An aliquot was removed for a zero time point before $MgCl_2$ in TES was added to initiate the cleavage reaction (at 25°C). Final concentrations in the cleavage reactions were 40 mM Tris–HCl (pH 7.5), 1 mM EDTA, 0.5 mM spermidine and [$MgCl_2$] necessary for a final [Mg^{2+}] given in the text assuming stoichiometric chelation by the EDTA. Aliquots of the reactions were removed and stopped with an equal volume of formamide stop mix containing 100 mM EDTA. The products of the cleavage reactions were separated by electrophoresis on 6% polyacrylamide gels containing 7 M urea. The gels were dried, and the fraction of precursor cleaved was quantified using a Storm 820 Phosphorimager and ImageQuant software.

Rapid-mixing reactions were performed on a Chemical-Quench-Flow apparatus (KinTek Corporation Model RQF-3). Radiolabeled RNA was renatured and preincubated in TES as described above, and an aliquot was removed as a zero time point. Cleavage reactions were initiated by rapid mixing with a 2X solution of $MgCl_2$ or $CaCl_2$ in TES and quenched by rapid mixing with two volumes of EDTA (50 mM or higher depending on the [$MgCl_2$] or [$CaCl_2$]). Final concentrations in the cleavage reactions were 40 mM Tris–HCl (pH 7.5), 1 mM EDTA, 0.5 mM spermidine and $MgCl_2$ or $CaCl_2$ at various concentrations. To measure rates in lower concentrations of the divalent metal ion, the EDTA concentrations in the reactions were reduced to 0.1 mM. Aliquots of the quenched reactions were mixed with an equal volume of formamide and separated by electrophoresis on 6% polyacrylamide gels containing 7 M urea. The gels were dried, and the fraction of precursor cleaved was quantified as above.

Native gel electrophoresis

RNA samples from hand-mixing cleavage reactions were mixed with an equal volume of stop mix (15% glycerol and 100 mM EDTA) and separated on 6% polyacrylamide gels (37.5 to 1 acrylamide:bisacrylamide) run in 0.1 M Tris–acetate (pH 7.5) with 5 mM EDTA at low power (2.5 W) and low temperature (4°C) for 12–16 h. The gels were dried, and the fraction of precursor cleaved was quantified as above.

Preparation of 3′ end-labeled precursor RNA

RNA was labeled at the 3′ end with [5′-^{32}P]pCp (14,29). The [5′-^{32}P]pCp was prepared in a 25 µl reaction that contained 1 nmol of 3′ CMP, 100 pmol of [γ^{32}P]ATP and 30 U of T4 polynucleotide kinase in 50 mM Tris–HCl (pH 7.6), 10 mM $MgCl_2$ and 10 mM 2-mercaptoethanol; after incubation at 37°C for 30 min it was heated to 70°C for 5 min. Two micrograms of RNA were labeled in a 20 µl reaction containing 5 µl of the [5′-^{32}P]pCp and 10 U of T4

RNA Ligase in 50 mM Tris–HCl (pH 7.5), 10 mM $MgCl_2$, 10 mM DTT, 1 mM ATP and 0.06 mg/ml aceylated BSA. The labeling reaction was incubated at 37°C for 30 min and stopped by adding an equal volume of formamide containing 100 mM EDTA. The labeled RNA was gel purified, precipitated and stored in 0.1 mM EDTA at −20°C.

RNA structure mapping

For the alkaline hydrolysis ladder, 3′ end-labeled RNA in 50 mM $NaHCO_3$ (pH 9.0), 1 mM EDTA and 0.25 mg/ml yeast tRNA was heated for 2 min at 95°C. An equal volume of 4.5 M NaAcetate was added, and the RNA was ethanol precipitated. To generate a G-ladder, 3′ end-labeled RNA was denatured for 2 min at 95°C in a reaction containing 9 M Urea, 30 mM NaCitrate (pH 3.5), 1.5 mM EDTA and 0.3 mg/ml yeast tRNA. The reaction mix was then cooled to 55°C for 1 min before adding T1 ribonuclease to 5 U/ml. After incubating at 55°C for 30 min, the tubes were placed in dry ice. For T1 cutting under native conditions, 3′ end-labeled RNA was heated to 95°C for 2 min in 0.1 mM EDTA and then adjusted to 40 mM Tris–HCl (pH 7.5), 1 mM EDTA, 0.5 mM spermidine. The reaction mix was preincubated at 37°C for 15 min followed by 25°C for 10 min before T1 ribonuclease was added to 0.5 U/ml. After 30 min at 25°C, an equal volume of formamide with 100 mM EDTA was added and the tubes were placed in dry ice. The products of the alkaline hydrolysis, T1 sequencing, and T1 structure mapping reactions were separated by electrophoresis on 8% polyacrylamide gels containing 7 M urea.

Curve fitting

Nonlinear, least squares fitting with KaleidaGraph (Synergy Software) was used to plot and analyze the reaction kinetics and binding data. For the kinetics, fraction cleaved (f) at each time point (t) was fit to a first-order exponential equation, $f = F\ (1–e^{-k_{obs}(t)})$, to obtain the observed rate constant (k_{obs}) and an endpoint (F) for each reaction. Estimates of the k_{obs} of the slow phase were made from the slope of the line after the burst (divided by the remaining fraction of total precursor) or by fitting the complete data set to the sum of two exponential equations. For the metal concentration curves, a simple binding model is assumed where

$$R + n(M) <=> R \cdot M_n \text{ and } k_{obs} = k_{max} \times [R \cdot M_n]/[R]_{total}.$$

The apparent dissociation constant $K_{d,app} = [R][M]^n/[R{\cdot}M_n]$, and $k_{obs} = k_{max}/(1 + K_{d,app}/[M]^n)$. R is ribozyme without bound metal (M), n is the Hill coefficient and k_{max} is the rate constant for saturating [M].

RESULTS

Wild-type sequence upstream of the ribozyme affects both self-cleavage rate and extent of cleavage

In vitro self-cleavage activity of the PAH1 precursor, which contained the poly(A) sequence elements, was compared to the shorter ribozyme, PEX1 (Figure 1). The shorter PEX1 precursor cleaved with first-order kinetics and a rate constant (k_{obs}) of ~15 min^{-1} (in 10 mM Mg^{2+}, pH 7.5, 25°C) (Figure 2a). In this set of experiments, a higher endpoint was observed for data collected by hand mixing (~90%) than for data collected with the rapid quench instrument (~70%). However, when fit to a first-order exponential, both sets of data gave similar values for k_{obs}. Following addition of $MgCl_2$, slightly less than half of the PAH1 precursor cleaved in the first few

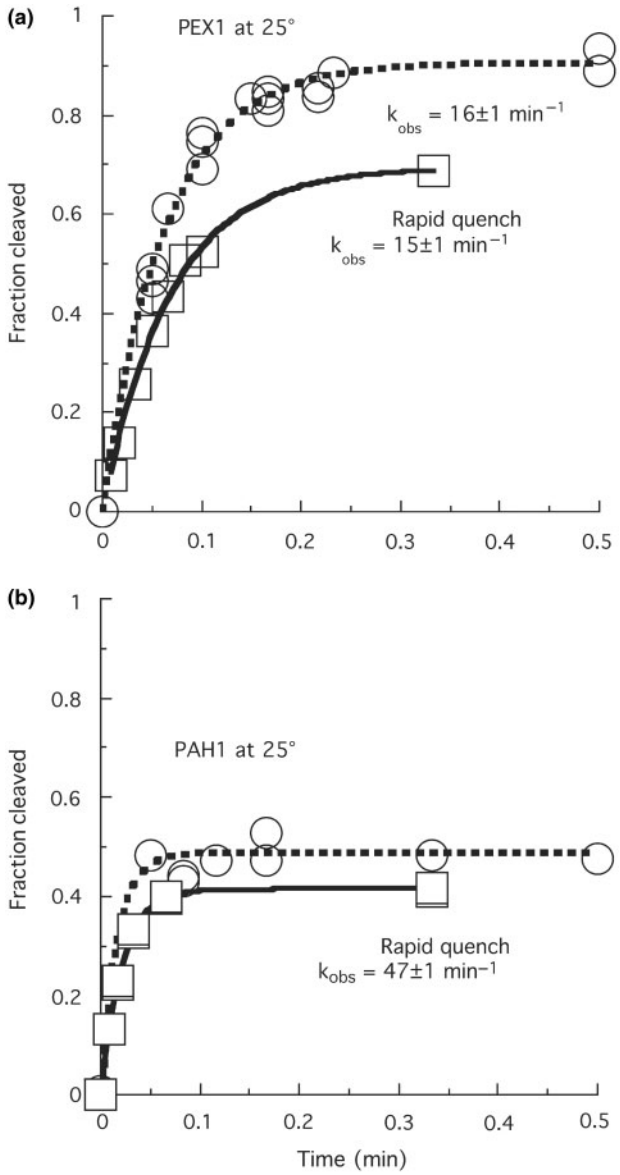

Figure 2. Upstream sequence alters the extent of reaction and the cleavage rate of the antigenomic ribozyme. (**a**) Cleavage of PEX1 precursor (25°C, 10 mM Mg^{2+}, pH 7.5). The data shown were collected both by hand mixing (circles, 90% cleaved) and on a rapid quench instrument (squares, 69% cleaved). In other experiments, with data collected manually, the extent of cleavage also ranged from 70% to 90% (data not shown). (**b**) Cleavage of PAH1 (25°C, 2 mM Mg^{2+}, pH 7.5). Data were collected manually (circles, 49% cleaved) and by rapid quench (squares, 42% cleaved). The first 30 s of 4 h reactions collected by hand are shown. The rate constant for cleavage in the slow phase was estimated to be no $>10^{-3} min^{-1}$. The rate constant for the initial reaction is reported only for the data collected on the rapid quench instrument.

seconds (Figure 2b), but there was little additional cleavage thereafter (some reactions were allowed to continue for up to 24 h, data not shown).

PAH1 appeared to form functionally distinct populations that were stable in a variety of reaction conditions. The endpoint of the PAH1 reactions did not increase with changes in [$MgCl_2$] (0.5 to 100 mM) or with the addition of NaCl (0.1–0.2 M). A variety of different preincubation conditions also failed to increase the extent of cleavage, and the 'slow-cleaving' fraction remained slow ($k_{obs} \leq 10^{-3}\,min^{-1}$ at 25°C). If, however, the reaction containing Mg^{2+} was briefly heated to 95°C after the initial phase at 25°C, most of the remaining precursor fraction did cleave (data not shown).

Although the extent of cleavage of PAH1 was lower than PEX1 under the same reaction conditions, the fraction that cleaved did so with a k_{obs} about three times higher than PEX1 (Figures 2a and b, and 3). We propose that roughly half of the PAH1 precursor adopted an active-ribozyme fold, and it may cleave faster than the shorter PEX1 precursor, while the remainder remained trapped in a kinetically stable inactive fold under the same reaction conditions. Two alternative explanations for a lower extent of cleavage are that the reaction reached equilibrium between cleavage and ligation, or that, in these reaction conditions, there is a parallel first-order reaction which does not lead to cleavage. The second scenario could account for the higher k_{obs} without the actual cleavage rate increasing. Reasons to rule out these two possibilities will be addressed in the discussion after additional data are presented. Finally, we note that there was no increase in the k_{obs} of PEX1 when the upstream fragment of RNA was isolated from a PAH1 transcription reaction and added in excess to a reaction with PEX1.

Metal ion dependence of the PAH1 ribozyme

To facilitate the comparison of the cleavage kinetics of PAH1 and PEX1 in manual mixing experiments, the $MgCl_2$ concentration was reduced to slow the reactions. In 1 mM Mg^{2+} at 25°C, the PAH1 ribozyme continued to cleave with a higher k_{obs} ($\geq 20\,min^{-1}$) (Figure 3) and still to ~50% (data not shown). A [Mg^{2+}]-rate curve for PAH1 cleavage revealed that, under the reaction conditions used (25°C, pH 7.5), the concentration of Mg^{2+} that gave one half k_{max} ($[M]_{1/2}$) was 1.2 ± 0.2 mM (Figure 3). This value was about 10-fold lower than the $[M]_{1/2}$ (~10 mM) for the PEX1 ribozyme as reported previously (30).

The PEX1 version of the antigenomic ribozyme cleaved faster in Ca^{2+} than in Mg^{2+} (31). Higher rates for PAH1 cleavage were also seen in reactions with Ca^{2+} where there was a 3-fold increase relative to those with Mg^{2+}. The $[M]_{1/2}$ for Ca^{2+} was also relatively low (1.7 ± 0.4 mM) (Figure 3). The low $[M]_{1/2}$ for Ca^{2+} and Mg^{2+} suggested that the active fold of PAH1 could have a higher affinity for metal ion than the shorter version, PEX1.

Stabilizing AltP2 reduced the extent of ribozyme cleavage

The extent of cleavage of PAH1 was less than that of the shorter precursor (PEX1) suggesting that wild-type sequence upstream (5′) of the cleavage site inhibited formation of an active ribozyme. In studies with the genomic sequence, Chadalavada *et al.* (15,16) found that a segment of 5′ sequence could form an alternative duplex with the 3′ end of the ribozyme. This new pairing prevented native ribozyme formation and inhibited cleavage. To test the hypothesis that the sequence upstream of the antigenomic ribozyme had a similar effect, we introduced sequence changes into PAH1 that would be predicted to alter the stability of the putative P(-1) and AltP2.

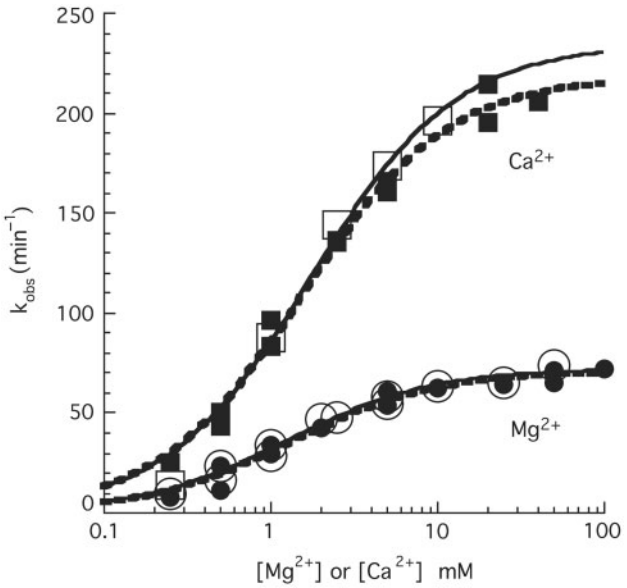

Figure 3. Dependence of cleavage rates on metal ion concentration. Cleavage of PAH1 (open symbols and solid lines) and PAH3 (closed symbols and dashed lines) was compared in Mg^{2+} and Ca^{2+}. Kinetic data were collected by rapid quench (the extent of cleavage was 40–50% for PAH1 and 70 to 85% for PAH3 in these reactions). The concentrations of Mg^{2+} (circles) and Ca^{2+} (squares) in the reactions were varied from 0.2 to 100 mM, and all reactions were at 25°C and pH 7.5. For PAH1 in Mg^{2+}, $k_{max} = 72 \pm 2\,min^{-1}$ and $K_{d,app} = 1.3 \pm 0.2$ mM; in Ca^{2+}, $k_{max} = 234 \pm 15\,min^{-1}$ and $K_{d,app} = 1.7 \pm 0.4$ mM. For PAH3 the corresponding values were $k_{max} = 71\,min^{-1}$, $K_{d,app} = 1.3$ mM (in Mg^{2+}) and $k_{max} = 218\,min^{-1}$, $K_{d,app} = 1.6$ mM (in Ca^{2+}).

Introducing additional base pairs to stabilize the alternative pairing (AltP2) would be predicted to reduce the extent of antigenomic ribozyme cleavage. PAH2, the construct with a stabilized AltP2 (Figure 4a) differed from PAH1 at five positions in the upstream sequence that could form the 5′ side of AltP2 (C-19a, C-21u, U-22c, G-23u and G-25u). With the PAH2 precursor, <1% of the RNA cleaved in the initial phase of the reaction (Figure 5a and b), and no additional specific cleavage was observed with longer incubation (≤2% after 4 and 24 h at 25°C, data not shown). Considering that no mutations were made in the ribozyme domain, this result was consistent with the hypothesis that the formation of an alternate pairing (such as a stabilized AltP2) inhibited ribozyme activity in PAH2.

Stabilizing P(-1) increased the extent of ribozyme cleavage

Two constructs predicted to have more stable P(-1) structures, PAH3 and PAH4, were also tested. In PAH3,

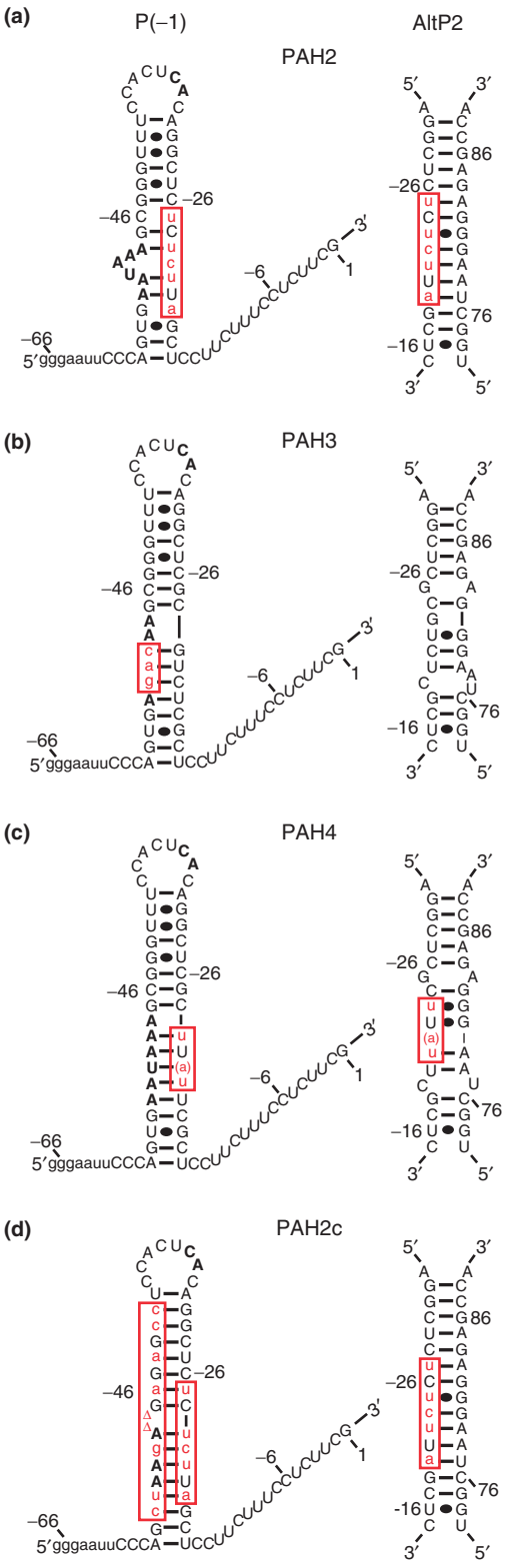

Figure 4. Potential secondary structures of P(-1) and AltP2 in the modified precursors. Sequences and hypothetical secondary structures are presented for just the P(-1) and AltP2 of (**a**) PAH2, (**b**) PAH3, (**c**) PAH4 and (**d**) PAH2c. Red letters in the boxed areas denote the mutations made in the wt 5′ leader sequence. Nucleotide numbering is as in PAH1 (Figure 1) and was not modified to account for nucleotide insertions and deletions that were introduced into the variants.

3 base changes (A-50c, U-51a and A-52g) were introduced into the 5′ side of the proposed P(-1) (Figure 4b). These changes were predicted to increase the number of base pairs in P(-1). Precursor RNA from this construct cleaved to >75% (Figure 5a and b). The k_{obs} for cleavage of PAH3 in either Mg^{2+} or Ca^{2+} were indistinguishable from those

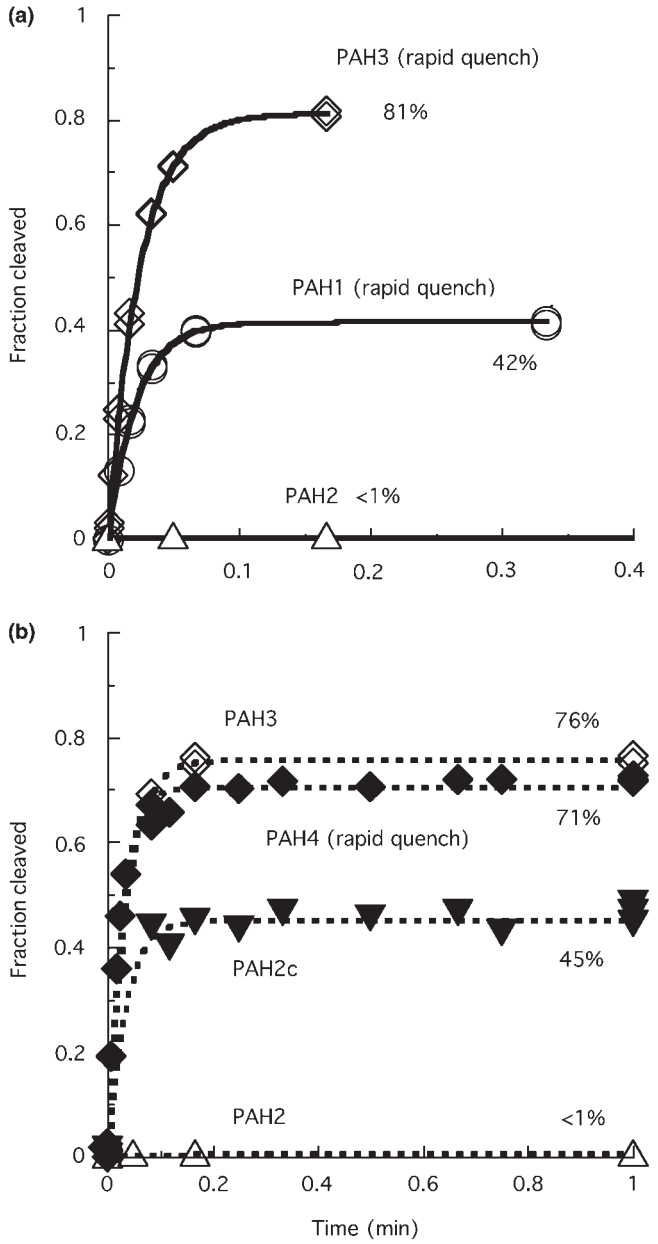

Figure 5. Changes in the upstream (5′) sequence can alter the extent of self-cleavage. (**a**) Cleavage of PAH2 (triangles) and PAH3 (diamonds) compared to the wt PAH1 (circles). The data for PAH3 (and PAH1) were collected on a rapid quench instrument. PAH2 cleavage was nearly undetectable. PAH3 cleaved to 81% with a rate constant ($42 \pm 2\,min^{-1}$) that was similar to PAH1 ($47 \pm 2\,min^{-1}$). Reaction conditions were 2 mM Mg^{2+}, pH 7.5 and 25°C. (**b**) Cleavage of PAH4 (closed diamonds) and PAH2c (closed inverted triangles). PAH4 data collected by rapid quench generated rate constants of $41 \pm 2\,min^{-1}$. Data for PAH2, PAH3 and PAH2c for this experiment were collected by hand mixing, so only the extent of cleavage could be determined in those reactions.

of the self-cleaving fraction of the original PAH1 (Figure 3). Thus, the only apparent difference between the cleavage kinetics of PAH3 and PAH1 was the greater extent of cleavage of the PAH3 RNA. In PAH4, mutations were introduced in the 3′ side of P(-1) to again increase base pairing in P(-1) (C-21u, G-23u and insertion of an A between −22/−21; Figure 4c). PAH4 behaved much like PAH3; in Mg^{2+} it cleaved to ~70% with a $k_{max} = 71 \pm 3\,min^{-1}$ (Figure 5b) and a $[M]_{1/2} = 1.6 \pm 0.2\,mM$ (data not shown).

The results from these studies with both PAH3 and PAH4 supported the idea that stabilizing the P(-1) hairpin structure in the 5′ sequence somehow favored the formation of the active ribozyme structure. Cleavage activity was the same when changes were made to either the 5′ or 3′ side of the predicted P(-1) suggesting that the P(-1) structure, more so than its sequence, contributed to this effect.

P(-1) competes with AltP2

According to the proposed pairing schemes, P(-1) and AltP2 share a common sequence. If so, it should be possible to restore a higher extent of cleavage in a precursor with the PAH2 changes (which had increased base pairing in AltP2), by also increasing the number of potential base pairs in P(-1). A more stable P(-1) would be predicted to compete with the stabilized AltP2. Additional changes to PAH2 were introduced into only the 5′ side of P(-1) (U-41c, U-42c, G-44a, C-46a, A-48△, A-49△, U-51g, G-54u and U-55c) (Figure 4d). In this construct (PAH2c), both P(-1) and AltP2 were capable of more extensive base pairing than the starting PAH1 sequence. Consistent with the prediction, these changes increased cleavage of the precursor RNA from the 1% seen in PAH2 to 45 ± 5% (PAH2c, Figure 5b). The reaction was too fast to extract a rate constant from data collected in hand-mixing experiments; however, PAH2c cleaved faster than PEX1, and probably as fast as PAH1.

Active and inactive conformations were resolved by nondenaturing polyacrylamide gel electrophoresis

Four of the precursor RNAs, PAH1, 2, 3 and 4, were analyzed by nondenaturing polyacrylamide gel electrophoresis (Figure 6). Prior to loading, the RNA either received no additional treatment after thawing, or the RNA was heated and renatured as for the cleavage reactions. In a third sample, Mg^{2+} was added to the renatured precursors for 1 min before EDTA was added to stop the reaction. The untreated wild-type precursor RNA (PAH1) ran as a diffuse set of two darker bands and at least one additional much lighter band (noted with asterisks, Figure 6). After renaturation, there was a change in distribution within that set, and the faster-migrating band was most abundant (asterisk 1). This darker band was identified as the active ribozyme species because it decreased in intensity with Mg^{2+} treatment, and two new fast migrating product bands appeared. About half of the total amount of precursor cleaved (~54% in the example shown). There was no noticeable change in the intensity of the slower migrating precursor band, and thus, it appeared to be an inactive form (asterisk 2). It is also noted that these data reveal that the precursor RNA adopted these different folds prior to the addition of Mg^{2+}.

Precursors PAH2, PAH3 and PAH4 were resolved under the same conditions used for PAH1 (Figure 6). The poorly cleaving PAH2 RNA ran predominantly in the position of the slower of the two dark precursor bands after the renaturation step (asterisk 2), and little, if any, cleaved when Mg^{2+} was added. The better-cleaving PAH3 and PAH4 precursors migrated predominantly in two bands if untreated (asterisks 1 and 2). However, after the renaturation step, most of the RNA had converted to the faster species (asterisk 1). This band disappeared with the addition of Mg^{2+} and two faster migrating bands appeared, suggesting it had cleaved. These data were entirely consistent with the interpretation that

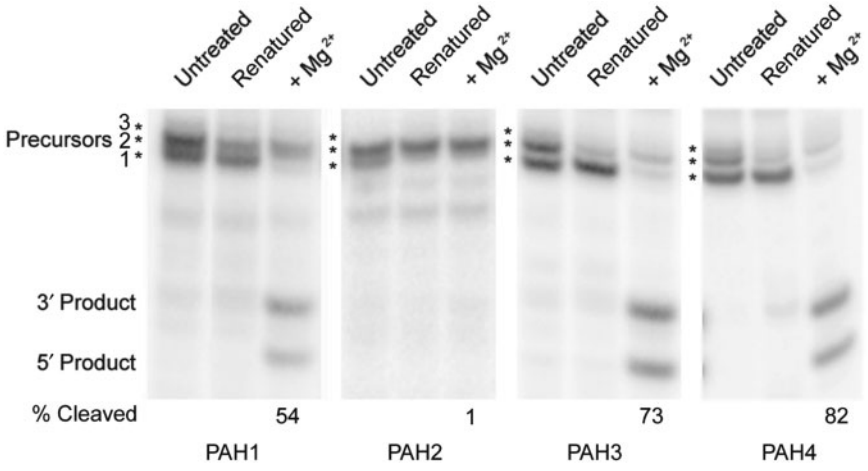

Figure 6. Nondenaturing polyacrylamide gel electrophoresis. Migrations of PAH1, PAH2, PAH3 and PAH4 precursors are shown (left to right panels, respectively). The RNA either received no renaturation treatment (lanes labeled Untreated) or it was heated and renatured as in the cleavage reactions (lanes labeled renatured and $+Mg^{2+}$). The reactions with Mg^{2+} (2 mM) were terminated with EDTA after 1 min and the percent conversion to product is given below the image. Asterisks mark positions of the two darker and one faint precursor bands referred to in the text.

stabilization of P(-1) (PAH3 and PAH4) enhanced formation of the active ribozyme, while stabilization of AltP2 (PAH2) favored a structure incapable of cleavage. Importantly, the results suggest that the base changes predicted to increase pairing in P(-1) or AltP2 stabilized conformations that had mobility similar to those that formed with the wt PAH1 sequence.

Structure in the 5′ leader sequence

Ribonuclease T1 (a probe for unpaired Gs) was used to test for structure in the 5′ leader sequences of 3′ end-labeled PAH1(C76U), PAH2(C76U), PAH3(C76U) and PAH4(C76U) precursor RNAs. (The inactive C76U variant of the ribozyme was used to prevent self-cleavage of the precursor under structure mapping conditions.) Under denaturing conditions, T1 cleaved, to a similar extent, at all Gs in the 5′ leader sequences of all four constructs (Figure 7a). Under conditions favorable for secondary structure formation, T1 cleavage in the wild-type 5′ leader sequence was reduced at −25, −29, −30, −43, −44, −45 and −47. This protection would be consistent with the formation of the upper portion of the predicted P(-1) structure (Figure 7b). The Gs at −54 and −56 remained accessible to T1 suggesting that either the short stem below the bulge in P(-1) did not form or that its formation was transient under these conditions. While these data were consistent with a structured 5′ leader that includes the upper duplex of the predicted P(-1), structure probing data cannot eliminate other potential alignments.

We next examined the T1 cleavage patterns in the 5′ leader sequences of PAH2(C76U), PAH3(C76U) and PAH4(C76U). In the PAH2(C76U) precursor, under non-denaturing conditions, the Gs at −43, −44, −45, −47, −54 and −56 in the 5′ side of P(-1) were all accessible to T1 cutting, whereas positions −23, −25, −29 and −30 in the 3′ side of P(-1) were protected. This pattern was consistent with the disruption of P(-1) and the formation of an alternative structure that involves the 3′ side of P(-1), such as AltP2. In PAH3(C76U) and PAH4(C76U), all of the Gs in the 5′ leader were protected from T1 cutting in nondenaturing conditions. This result was consistent with the formation of a stabilized P(-1) structure that includes the upper stem that forms in the wild-type PAH1(C76U), as well as base pairs involving nucleotides in the bulge and at the base of P(-1) that did not appear to form stable pairing interactions in the wild-type construct.

DISCUSSION

During synthesis of the antigenomic RNA sequence of HDV, ribozyme cleavage and mRNA 3′ processing may be competing events. To test if antigenomic HDV ribozyme activity might be influenced by upstream sequences near the poly(A) site, we have examined a ribozyme precursor that included an additional 60 nt of 5′ sequence. Evidence that the upstream sequence alters ribozyme activity was

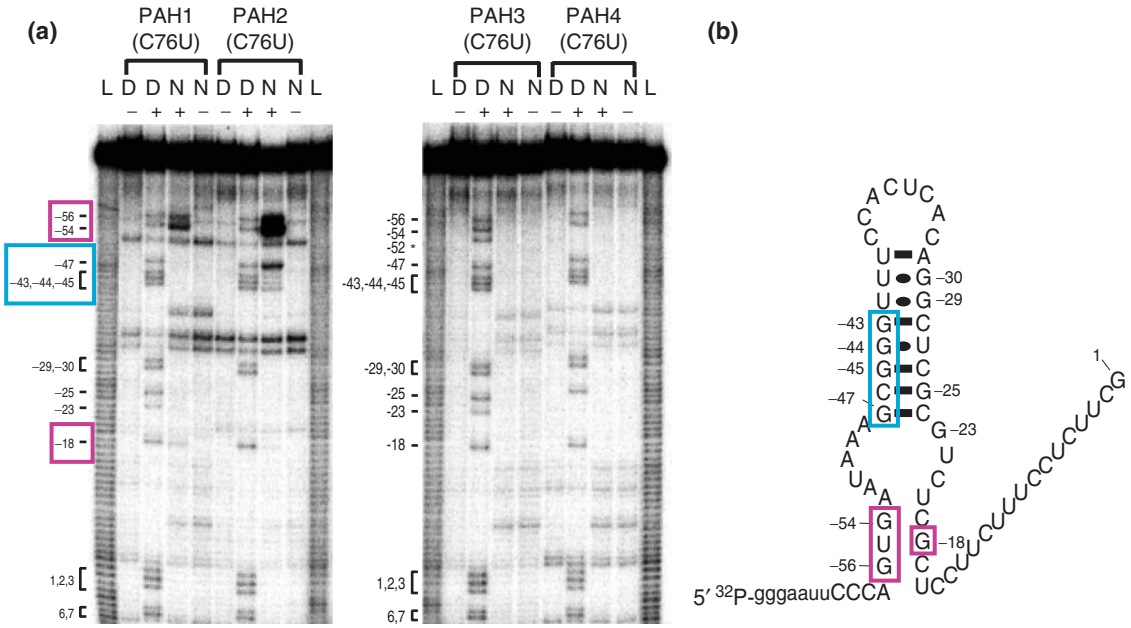

Figure 7. Ribonuclease T1 structure mapping of 5′ leader sequence in PAH1(C76U), PAH2(C76U), PAH3(C76U), and PAH4(C76U). (**a**) 3′ end-labeled precursor RNA was digested with ribonuclease T1 under denaturing and nondenaturing conditions. Numbered positions correspond to nucleotides in PAH1 (Figure 1). Lanes are labeled according to treatment conditions: (L) Hydrolysis Ladder, (D) Denaturing conditions − or +T1, (N) Nondenaturing conditions − or + T1. (**b**) Secondary structure of P(-1). Base pairs that form the upper part of P(-1) are supported by T1 structure mapping data for PAH1(C76U), whereas potential base pairs that could form a short stem at the base of P(-1) are not. The magenta boxes highlight Gs in PAH1(C76U) and PAH2(C76U) that are accessible to T1 in both denaturing and nondenaturing conditions. The blue box corresponds to Gs that are cut by T1 in both denaturing and nondenaturing conditions only in the PAH2(C76U) construct. All other Gs are accessible in denaturing conditions, but are resistant to T1 cleavage in nondenaturing conditions.

seen in the ribozyme cleavage rate profile in that the extent of the reaction was reduced to ~50%. The extent of cleavage in several precursor variants correlated with the potential for base pairing between two competing structural elements, whereas the increase in the observed cleavage rate of the active fraction appeared largely unaffected by sequence changes in those same regions. In all constructs tested, the slow-cleaving fraction was remarkably stable in $MgCl_2$-containing buffers at 25°C; cleavage of that fraction was estimated to be at least 10^4-fold slower than cleavage of the more active fraction.

Previous studies with a genomic HDV ribozyme construct similar in length to PAH1 used here, revealed biphasic kinetics where 36% of the RNA cleaved fast ($51\,min^{-1}$) and the remainder cleaved slowly ($0.13\,min^{-1}$) (conditions were 37°C, 10 mM Mg^{2+}, pH 8.0) (32). The cleavage profile for the antigenomic PAH1 construct used in our studies (50% cleaved) can also be viewed as biphasic but with a very slow second phase. Alternatively, a reaction profile that levels off without the going to completion could result from an approach to equilibrium between cleaved and religated RNA. If correct, the equilibrium explanation for the kinetic profile would be exciting because ligation of ribozyme cleavage products by the HDV ribozymes, in a reverse reaction, has not been demonstrated. Indeed, invoking a role for AltP2 in bringing the 5′ and 3′ ends of the linear cleavage products together for ligation could be an attractive solution to the biological problem of circularizing the unit-length RNA during HDV replication (2,3). However, the endpoint of ~50% seen with the PAH1 precursor does not appear to be the result of ligation activity. Varying the RNA concentration did not change the endpoint, nor were precursors regenerated from isolated products (unpublished data). More compelling, however, is that in the native gel analysis, differently folded populations of the precursor formed prior to the addition of Mg^{2+} to the reaction, and only one of those populations cleaved when Mg^{2+} was added.

Another possible explanation for the lower endpoint is that two parallel first-order reactions occurred upon the addition of Mg^{2+}. One pathway leading to ribozyme cleavage and the other one resulting in a stable noncleaving structure. If these two reactions proceeded with the same rate constant and drew from the same pool of precursor RNA, only half the RNA would be cleaved but the k_{obs} for the disappearance of precursor would be twice the rate constant for the cleavage pathway. Two independent lines of evidence argue against this model. First, the data from the native gels mentioned above was also incompatible with this model. Second, mutations that stabilized P(-1) in PAH3 and PAH4 increased the extent of cleavage but the k_{obs} did not return to the lower k_{obs} value of PEX1, as the parallel pathways model would have predicted.

The data presented here are most consistent with the idea that there are kinetically stable populations of alternatively folded poly(A) site-containing precursor RNA. In one population, a pairing such as AltP2 can turn-off ribozyme activity by preventing the active structure from forming. In the other population, a feature of the upstream sequence affects the native ribozyme structure in a manner that leads to the higher observed rate. This *in vitro* behavior could be consistent with a model in which interactions between sequences associated with the poly(A) region and the ribozyme influence relative usage of the two processing sites.

Chadalavada *et al.* (15,16) have shown that, in the genomic HDV ribozyme, sequences upstream of the cleavage site interact with ribozyme sequence. In the antigenomic sequence, however, sequence covariation in individual isolates of HDV did not strongly support unique alignments of base pairs in P(-1) and AltP2 (18). Multiple pairing alignments of the sequences appear possible, and P(-1) and AltP2 may thus represent examples of potential secondary structures involving the 5′ sequences. Moreover, in this case, mutations and compensatory mutations do not necessarily define the true competing secondary structures because the assay only reports that another structure was prevented from forming correctly. Thus, while the evidence is consistent with the hypothesis that AltP2 will interfere with ribozyme activity, it is not possible to say with certainty that interference of ribozyme activity is due to formation of AltP2 exactly as drawn. This uncertainty is not due to a lack of structural data, but to the nature of the activity assay. Despite this uncertainty, mutations predicted to increase AltP2 stability decreased the extent of cleavage, as was the prediction. Moreover, a more stable P(-1)-like structure predicted to compete with AltP2 increased the fraction of precursor that cleaved. Base pairing, but not a specific sequence, in P(-1) appeared to be the important feature that enhanced the extent of cleavage.

The k_{obs} for PAH1 cleavage at 25°C (~1–4 s^{-1}, depending on metal ions) was higher than previously seen with the shorter ribozymes from HDV. Nevertheless, the increase relative to PEX1 was modest (~3-fold). This increase might not be another example of flanking 'extra-ribozyme' sequences (or domains) that stabilize the core ribozyme. More dramatic examples of that effect on the k_{obs} for cleavage in small ribozymes have been seen with extended versions of the hairpin (33), hammerhead (34) and *glmS* ribozymes (35–37). In these ribozymes, where flanking sequences stabilize an active structure, the rate enhancements are typically much larger, and the extra sequence makes an obvious structural contribution. For the wild-type PAH1 ribozyme or the PAH3 and PAH4 variants, interactions that could contribute to the stability of the HDV ribozyme core are not apparent. Chadalavada *et al.* (15,16) observed a similar increase in k_{obs} of the genomic HDV ribozymes with extra 5′ sequence. They have described a statistical mechanical model based on the rapid interchange of tertiary structures between native (active) and inactive forms under cleavage conditions (32). That model, also applicable to the antigenomic HDV ribozymes, would predict that k_{obs} for PAH1 or PEX1 was less than the rate determining k_{cat} for self-cleavage because only a statistical fraction, f_3, of the folded ribozyme precursor is in the native tertiary fold and capable of cleavage: that is, $k_{obs} = f_3 \times k_{cat}$. An increase in k_{obs} for PAH1 (and PAH3 and 4), relative to PEX1, could then reflect an increase in f_3 rather than an increase in k_{cat} for those ribozymes. Although the general model may explain

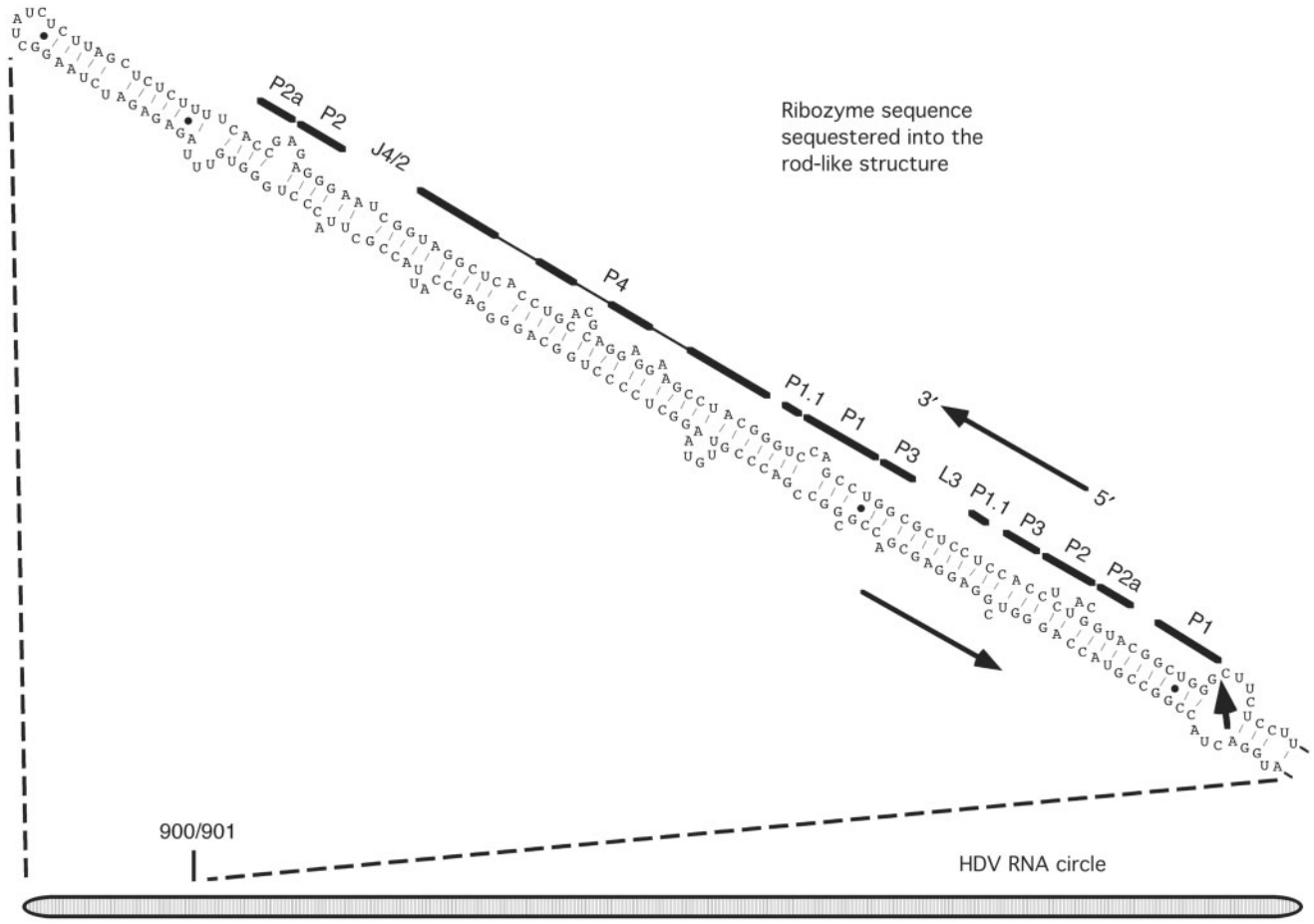

Figure 8. The ribozyme is near the end of the rod-like HDV antigenomic RNA. A cartoon of the circular single-stranded antigenomic RNA is presented at the bottom in its proposed rod-like structure. The ribozyme sequence (upper portion) is located near one end of the rod, and the locations of the paired elements in the antigenomic ribozyme are labeled. The cleavage site at the 5′ end of P1 is between nucleotides 901 and 900 in the viral numbering system (13). It should be noted that the sequence that pairs with the antigenomic ribozyme sequence is the template for the genomic ribozyme.

the change in k_{obs}, our data do not address a basis for the predicted change in f_3.

The potential for rapid ribozyme self-processing along with formation of stable nonribozyme structures could be important to the biology of the virus. The sequence coding for the ribozyme is near one end of a duplex rod formed by base pairing in the HDV RNA (Figure 8). Rapid cleavage of the ribozyme during replication may ensure that the ribozyme acts very soon after it is synthesized. If not, a large hairpin that forms at the end of the rod-like structure could sequester the uncleaved ribozyme sequence (Figure 8) leading to the accumulation of primary replication products. Assuming a transcription rate of about 10–20 nt/s, a slow-cleaving ribozyme sequence could be sequestered as an inactive duplex within 5–10 s after the completion of the ribozyme domain. Although such pairing could prevent unwanted re-cleavage by the ribozyme after the circles are generated, it would presumably interfere with processing of the initial transcript (2,38,39). With a half-life on the order of 1 s, a newly synthesized ribozyme could cleave before the polymerase transcribes around the hairpin end of the circular genomic RNA. The flip side, however, is that high ribozyme activity during transcription of the mRNA could reduce polyadenylation efficiency. Such an effect could occur even though the ribozyme is downstream of the poly(A) site (6,7). Thus, inhibition of ribozyme activity under some conditions may be required for efficient polyadenylation and mRNA maturation. A need to suppress ribozyme self-cleavage, under certain conditions, may not be unique to the virus. Recently, a sequence coding for an active HDV-like ribozyme was discovered in the mammalian gene for CPEB3 (cytoplasmic polyadenylation element binding protein 3) (40). Even though that ribozyme is located in an intron, self-cleavage of the RNA might interfere with or alter CPEB3 expression if cleavage was faster than splicing.

ACKNOWLEDGEMENTS

We thank Feng Su and Sara Wilkinson for comments on earlier versions of this manuscript. This work was supported by National Institutes of Health (GM047233). Funding to pay the Open Access publication charges for this article was provided by NIH grant GM047233.

Conflict of interest statement. None declared.

REFERENCES

1. Branch,A.D. and Robertson,H.D. (1984) A replication cycle for viroids and other small infectious RNA's. *Science*, **223**, 450–455.
2. Taylor,J.M. (1992) The structure and replication of hepatitis delta virus. *Annu. Rev. Microbiol.*, **46**, 253–276.
3. Lai,M.M. (1995) The molecular biology of hepatitis delta virus. *Annu. Rev. Biochem.*, **64**, 259–286.
4. Hsieh,S.Y., Chao,M., Coates,L. and Taylor,J. (1990) Hepatitis delta virus genome replication: a polyadenylated mRNA for delta antigen. *J. Virol.*, **64**, 3192–3198.
5. Hsieh,S.Y. and Taylor,J. (1991) Regulation of polyadenylation of hepatitis delta virus antigenomic RNA. *J. Virol.*, **65**, 6438–6446.
6. Bird,G., Fong,N., Gatlin,J.C., Farabaugh,S. and Bentley,D.L. (2005) Ribozyme cleavage reveals connections between mRNA release from the site of transcription and pre-mRNA processing. *Mol. Cell*, **20**, 747–758.
7. Rigo,F., Kazerouninia,A., Nag,A. and Martinson,H.G. (2005) The RNA tether from the poly(A) signal to the polymerase mediates coupling of transcription to cleavage and polyadenylation. *Mol. Cell*, **20**, 733–745.
8. Macnaughton,T.B., Shi,S.T., Modahl,L.E. and Lai,M.M. (2002) Rolling circle replication of hepatitis delta virus RNA is carried out by two different cellular RNA polymerases. *J. Virol.*, **76**, 3920–3927.
9. Nie,X., Chang,J. and Taylor,J.M. (2004) Alternative processing of hepatitis delta virus antigenomic RNA transcripts. *J.Virol.*, **78**, 4517–4524.
10. McCracken,S., Fong,N., Yankulov,K., Ballantyne,S., Pan,G., Greenblatt,J., Patterson,S.D., Wickens,M. and Bentley,D.L. (1997) The C-terminal domain of RNA polymerase II couples mRNA processing to transcription. *Nature*, **385**, 357–361.
11. Calvo,O. and Manley,J.L. (2003) Strange bedfellows: polyadenylation factors at the promoter. *Genes Dev.*, **17**, 1321–1327.
12. Modahl,L.E., Macnaughton,T.B., Zhu,N., Johnson,D.L. and Lai,M.M. (2000) RNA-Dependent replication and transcription of hepatitis delta virus RNA involve distinct cellular RNA polymerases. *Mol. Cell Biol.*, **20**, 6030–6039.
13. Kuo,M.Y., Sharmeen,L., Dinter-Gottlieb,G. and Taylor,J. (1988) Characterization of self-cleaving RNA sequences on the genome and antigenome of human hepatitis delta virus. *J. Virol.*, **62**, 4439–4444.
14. Perrotta,A.T. and Been,M.D. (1990) The self-cleaving domain from the genomic RNA of hepatitis delta virus: sequence requirements and the effects of denaturant. *Nucleic Acids Res.*, **18**, 6821–6827.
15. Chadalavada,D.M., Knudsen,S.M., Nakano,S. and Bevilacqua,P.C. (2000) A role for upstream RNA structure in facilitating the catalytic fold of the genomic hepatitis delta virus ribozyme. *J. Mol. Biol.*, **301**, 349–367.
16. Chadalavada,D.M., Senchak,S.E. and Bevilacqua,P.C. (2002) The folding pathway of the genomic hepatitis delta virus ribozyme is dominated by slow folding of the pseudoknots. *J. Mol. Biol.*, **317**, 559–575.
17. Colgan,D.F. and Manley,J.L. (1997) Mechanism and regulation of mRNA polyadenylation. *Genes Dev.*, **11**, 2755–2766.
18. Wadkins,T.S. and Been,M.D. (2002) Ribozyme activity in the genomic and antigenomic RNA strands of hepatitis delta virus. *Cell. Mol. Life Sci.*, **59**, 112–125.
19. Pan,J. and Woodson,S.A. (1998) Folding intermediates of a self-splicing RNA: mispairing of the catalytic core. *J. Mol. Biol.*, **280**, 597–609.
20. Berkhout,B., Klaver,B. and Das,A.T. (1995) A conserved hairpin structure predicted for the poly(A) signal of human and simian immunodeficiency viruses. *Virology*, **207**, 276–281.
21. Das,A.T., Klaver,B. and Berkhout,B. (1999) A hairpin structure in the R region of the human immunodeficiency virus type 1 RNA genome is instrumental in polyadenylation site selection. *J. Virol.*, **73**, 81–91.
22. Klasens,B.I., Thiesen,M., Virtanen,A. and Berkhout,B. (1999) The ability of the HIV-1 AAUAAA signal to bind polyadenylation factors is controlled by local RNA structure. *Nucleic Acids Res.*, **27**, 446–454.
23. Davanloo,P., Rosenberg,A.H., Dunn,J.J. and Studier,F.W. (1984) Cloning and expression of the gene for bacteriophage T7 RNA polymerase. *Proc. Natl Acad. Sci. USA*, **81**, 2035–2039.
24. Perrotta,A.T., Nikiforova,O. and Been,M.D. (1999) A conserved bulged adenosine in a peripheral duplex of the antigenomic HDV self-cleaving RNA reduces kinetic trapping of inactive conformations. *Nucleic Acids Res.*, **27**, 795–802.
25. Perrotta,A.T. and Been,M.D. (1992) Cleavage of oligoribonucleotides by a ribozyme derived from the hepatitis delta virus RNA sequence. *Biochemistry*, **31**, 16–21.
26. Kunkel,T.A., Roberts,J.D. and Zakour,R.A. (1987) Rapid and efficient site-specific mutagenesis without phenotypic selection. *Methods Enzymol.*, **154**, 367–382.
27. Vieira,J. and Messing,J. (1987) Production of single-stranded plasmid DNA. *Methods Enzymol.*, **153**, 3–11.
28. Perrotta,A.T. and Been,M.D. (1991) A pseudoknot-like structure required for efficient self-cleavage of hepatitis delta virus RNA. *Nature*, **350**, 434–436.
29. Bruce,A.G. and Uhlenbeck,O.C. (1978) Reactions at the termini of tRNA with T4 RNA ligase. *Nucleic Acids Res.*, **5**, 3665–3677.
30. Perrotta,A.T. and Been,M.D. (2007) A single nucleotide linked to a switch in metal ion reactivity preference in the HDV ribozymes. *Biochemistry*, **46**, 5124–5130.
31. Shih,I.H. and Been,M.D. (1999) Ribozyme cleavage of a 2,5-phosphodiester linkage: mechanism and a restricted divalent metal-ion requirement. *RNA*, **5**, 1140–1148.
32. Brown,T.S., Chadalavada,D.M. and Bevilacqua,P.C. (2004) Design of a highly reactive HDV ribozyme sequence uncovers facilitation of RNA folding by alternative pairings and physiological ionic strength. *J. Mol. Biol.*, **341**, 695–712.
33. Walter,F., Murchie,A.I. and Lilley,D.M. (1998) Folding of the four-way RNA junction of the hairpin ribozyme. *Biochemistry*, **37**, 17629–17636.
34. Khvorova,A., Lescoute,A., Westhof,E. and Jayasena,S.D. (2003) Sequence elements outside the hammerhead ribozyme catalytic core enable intracellular activity. *Nat. Struct. Biol.*, **10**, 708–712.
35. Winkler,W.C., Nahvi,A., Roth,A., Collins,J.A. and Breaker,R.R. (2004) Control of gene expression by a natural metabolite-responsive ribozyme. *Nature*, **428**, 281–286.
36. Wilkinson,S.R. and Been,M.D. (2005) A pseudoknot in the 3′ non-core region of the glmS ribozyme enhances self-cleavage activity. *RNA*, **11**, 1788–1794.
37. Roth,A., Nahvi,A., Lee,M., Jona,I. and Breaker,R.R. (2006) Characteristics of the glmS ribozyme suggest only structural roles for divalent metal ions. *RNA*, **12**, 607–619.
38. Lazinski,D.W. and Taylor,J.M. (1995) Intracellular cleavage and ligation of hepatitis delta virus genomic RNA: regulation of ribozyme activity by cis-acting sequences and host factors. *J. Virol.*, **69**, 1190–1200.
39. Lazinski,D.W. and Taylor,J.M. (1995) Regulation of the hepatitis delta virus ribozymes: to cleave or not to cleave? *RNA*, **1**, 225–233.
40. Salehi-Ashtiani,K., Luptak,A., Litovchick,A. and Szostak,J.W. (2006) A genomewide search for ribozymes reveals an HDV-like sequence in the human CPEB3 gene. *Science*, **313**, 1788–1792.